

TECHNICAL RESEARCH REPORT

A Practical Transmission System Based on the Human
Visual Model for Satellite Channels

by Junfeng Gu, Yimin Jiang, John S. Baras

CSHCN T.R. 99-6
(ISR T.R. 99-14)



The Center for Satellite and Hybrid Communication Networks is a NASA-sponsored Commercial Space Center also supported by the Department of Defense (DOD), industry, the State of Maryland, the University of Maryland and the Institute for Systems Research. This document is a technical report in the CSHCN series originating at the University of Maryland.

Web site <http://www.isr.umd.edu/CSHCN/>

A Practical Video Transmission System Based on Human Visual Model for Satellite Channel

Junfeng Gu *, Yimin Jiang +, John S. Baras *

* Institute for Systems Research, University of Maryland, College Park, MD 20742, USA

+ Hughes Network Systems Inc., 11717 Exploration Lane, Germantown, MD 20876, USA

Tel: +1-301-601-6494, Fax: +1-301-428-7177, Email: yjiang@hns.com

Abstract: This paper presents a practical architecture for joint source-channel coding of human visual model based video transmission over satellite channel. Perceptual distortion model just-noticeable-distortion (JND) is applied to improve the subjective quality of compressed videos. 3-D wavelet decomposition can remove spatial and temporal redundancy and provide scalability of video quality. In order to conceal the errors occurred under bad channel conditions, a novel slicing method and a joint source channel coding scenario that combines RCPC with CRC and utilizes the distortion information to allocate convolutional coding rates are proposed. A new performance index based on JND is proposed and used to evaluate the overall performance at different signal to noise ratios (SNR). Our system uses OQPSK modulation scheme.

I. INTRODUCTION

High quality video broadcasting via satellite channel is of great interests nowadays. In this paper we focus on a satellite video transmission system that combines human visual model, 3-D wavelet subband decomposition and joint source channel coding scheme.

Because the ultimate objective of video transmission systems is to maintain the subjective visual quality of images, performance metrics (other than MSE or PSNR) that take the psychovisual properties of human visual system (HVS) into account are proposed [5]. Several modern human visual models are developed, such as just-noticeable-distortion (JND) [5][12], visible difference predictor (VDP) [8] and three-component image model [9]. The JND model provides each pixel with a threshold of error visibility, below which reconstruction errors are rendered imperceptible. The JND profile of a video sequence is a function of local signal properties, such as brightness, background texture, luminance changes between two frames, and frequency distribution. Scalable video compression schemes (e.g. subband coding) are widely studied [1][3][4] because they allow selective transmission of subbands to different users depending on their quality

requirements and available channel bandwidths. Subband decomposition has extended to three dimensions (3-D) recently [1][2]. The JND model and 3-D wavelet decomposition are applied in our video codec. The quantizer is based on the JND model and to approach the perceptual optimum.

Traditionally source and channel coders are designed independently according to Shannon's source-channel separation theorem. However in any practical communication system with finite delay and finite complexity in source and channel coders there are advantages in joint source-channel coding. [15] gives a survey on recent progress on it.

In satellite broadcast case feedback channel is not available, thus the transmitter has no information about the receivers and their channel environments. It is difficult to guarantee the average video qualities under diversified channel conditions without large channel coding overhead. We derive a new slicing method to truncate the data from each subband into small slices before arithmetic coding. Rate compatible punctured convolutional (RCPC) codes [16] are adopted in our system. The advantage of using RCPC codes is that the high rate codes are embedded into the lower rate codes of the family and the same Viterbi decoder can be used for all codes of a family. Reed-Solomon code and Ramsay interleaver plus RCPC is used to protect the data from spatial LLLL temporal L subband. Cyclic redundancy check (CRC) codes are combined with RCPC for other less significant subbands to assure acceptable video quality even under bad channel conditions.

II THE JND MODEL BASED VIDEO CODEC

Figure 1 and Figure 2 show the JND model based video encoder and decoder respectively. In video encoder, the input video sequence is decomposed into eleven spatio-temporal frequency subbands in 3-D wavelet analysis module. The Frame Counter & Motion Detector renews the JND profiles from frame count and abrupt motion detection. The JND Model Generators estimate the

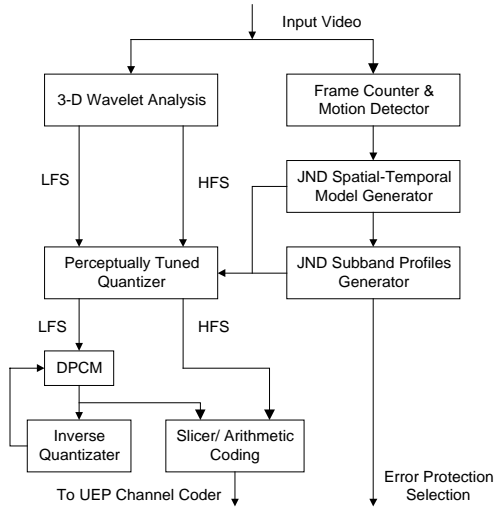


Figure 1 JND Based Video Encoder

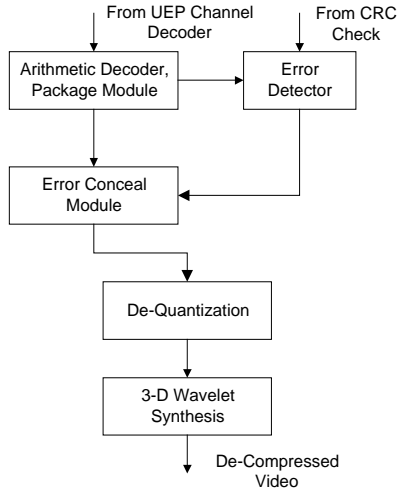


Figure 2 JND Based Video Decoder

spatio-temporal JND profile from analyzing local video signals and the distortion allocation algorithm that determines the JND profile for each subband. The Perceptually Tuned Quantizer quantizes the wavelet coefficients in each subband according to their JND profiles. The spatial LLLL temporal L subband will be encoded by DPCM. Then the data from all subbands goes through the Slicer and Arithmetic Coding part to do slicing and entropy coding. Afterward we get compressed video signal. Several modules in video codec will be presented subsequently.

1. 3-D Wavelet Analysis

The two-tap Haar wavelet is adopted to proceed temporal analysis, Antonini (7,9) wavelet [10] is used to proceed spatial analysis for the signal through the Haar filter. The temporal low frequency part is decomposed to

two levels, and high frequency part is decomposed to one level shown as Figure 3.

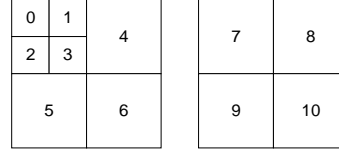


Figure 3 Subbands after 3-D Wavelet Decomposition

2. Frame Counter & Motion Detector

Because the calculation of the JND profiles is resource consuming, the Frame Counter & Motion Detector is designed to control the renew process of the JND. Typically the JND profiles are renewed every 10 to 20 frames, however they will be renewed immediately after an abrupt motion detected by a simple motion detector which calculates the energy of spatial LL temporal H subband (i.e. subband 7 in Figure 3). If the energy exceeds some threshold, an abrupt motion happens with high probability.

3. JND Model Generator

The JND provides each signal a threshold of visible distortion, below which reconstruction errors are rendered imperceptible. The JND profiles in spatio-temporal domain is as [6][7], we use the same syntax, please refer [6][7] for explanation:

$$JND_{s-t}(x, y, n) \equiv f_3(\text{ild}(x, y, n)) \cdot JND_s(x, y, n)$$

$$JND_s(x, y, n) \equiv \max\{f_1(\text{mg}(x, y, n)), f_2(\text{mg}(x, y, n))\} \quad (1)$$

$$0 \leq x < W, 0 \leq y < H$$

4. A Novel Human Perceptual Distortion Measure

Based on the basic concept of the JND, the idea of minimally-noticeable-distortion (MND) is developed for the situation that bit-rate budget is tight and the distortion in the reconstructed image is perceptually minimal at the available bit-rate and uniformly distributed over the whole image [12]. The perceptual quality of the reconstructed image is accordingly expected to degrade evenly if bit-rate is reduced. MND is expressed as:

$$MND(x, y) \equiv JND(x, y) \cdot d(x, y) \quad (2)$$

where $0 \leq x < W$, $0 \leq y < H$, W and H are the width and height of an image respectively, $d(x, y)$ is the distortion index at point (x, y) . We define the energy of MND of a small area indexed by (i, j) as:

$$\sum_{(x,y) \in r_{ij}} MND^2(x, y) \equiv \sum_{(x,y) \in r_{ij}} JND^2(x, y) \cdot \delta(i, j) \quad (3)$$

where r_{ij} is a small block (typically 8 by 8 pixels), $\delta(i, j)$ is the distortion index for this block. We can

define our global human perceptual distortion measure based on evaluating $\delta(i, j)$ as follows:

$$\Delta_G \equiv \frac{1}{KL} \sum_{k=1}^K \sum_{l=1}^L \varepsilon(k, l) \quad (4)$$

where $\varepsilon(k, l)$ is the distortion measure of a medium block indexed by (k, l) . We decompose the whole image into K by L non-overlapped medium blocks (R_{kl}); each medium block is divided into M by N small blocks ($r_{ij}(k, l)$), i.e., $R_{kl} = \bigcup_{i=1, M; j=1, N} r_{ij}(k, l)$.

$\varepsilon(k, l)$ is defined as:

$$\varepsilon(k, l) \equiv \text{median}(\delta(i, j) | r_{ij}(k, l) \in R_{kl}, 1 \leq i \leq M, 1 \leq j \leq N) \quad (5)$$

The larger Δ_G is, the larger the subjective perceptual distortion is. Compared with PSNR or MSE, Δ_G takes human visual model into account, therefore it can reflect the subjective visual quality better than PSNR or MSE. We will use this distortion measure to evaluate the performance of our system.

5. Perceptual Tuned Quantizer

The advantage of the JND model is that it provides a quantitative measure of the error sensitivity threshold with spatial and frequency localization. Therefore the quantization table based on the JND model can be localized, which adds a globally even control on the compressed video quality. A mid-rising uniform quantizer is adopted as our basic quantizer due to its simplicity and optimal performance under certain conditions [7][13].

First, the global object distortion index Δ_G is given, which typically ranges from 1.0 to 10.0, where 1.0 stands for just noticeable distortion. Second, each subband is partitioned into non-overlapped 8 by 8 blocks ($r_{ij}(k, l)$). For each block $r_{ij}(k, l)$, the step size of the quantizer is maximized under the condition that quantization error energy is less or equal to the MND energy in this block that has the distortion index $\delta(i, j)$ equal to Δ_G , i.e.,

$$\max \tau_{ij}(k, l) \left| \begin{array}{l} \sum_{(x, y) \in r_{ij}(k, l)} MND^2(x, y) \geq \sum_{(x, y) \in r_{ij}(k, l), w(x, y) < \tau_{ij}(k, l)} w(x, y)^2 + \\ \sum_{(x, y) \in r_{ij}(k, l), w(x, y) \geq \tau_{ij}(k, l)} [w(x, y) - \hat{w}(x, y)]^2 \end{array} \right. \quad (6)$$

where the energy of MND defined as (3), $w(x, y)$ is wavelet coefficient, $\hat{w}(x, y)$ is quantized wavelet coefficient. $\tau_{ij}(k, l)$ is the quantization step size of $r_{ij}(k, l)$. A quantization table that leads uniform error energy over all subbands is setup for each subband. It is

packaged in the header of the bit stream of this subband.

6. Arithmetic Coding and Slicing Algorithm

Arithmetic coding [14] is adopted to achieve efficient compression, however the decoding result of one coefficient depends on the decoding result of previous one because of adaptive coding procedure. In order to prevent decoding errors from spreading, a slicing algorithm is derived to truncate the whole subband into small bit streams before arithmetic coding. The idea is to make each such small bit stream carry the same amount of "distortion sensitivity". If we want to segment the subband S_i into I small bit streams, we can define I sets G of point (x, y) , such that for each set G_i ($i = 1, \dots, I$): $S_i = \bigcup_i G_i$ and

$$G_i = \left\{ (x, y) \left| \begin{array}{l} \sum_{(x, y) \in G_i} \frac{1}{JND^2(x, y)} = \frac{1}{I} \sum_{(x, y) \in S_i} \frac{1}{JND^2(x, y)} \\ (x, y) \in S_i, (x, y) \notin G_j, j \neq i \end{array} \right. \right\} \quad (7)$$

III. ERROR CONCEALMENT

1. Channel Model

The satellite channel can be well modeled as an additive white Gaussian noise (AWGN) channel; the received base-band time-domain signal is as follows:

$$y(t) = \sum_{n=0}^{N-1} [(a_n g(t - nT) + ja_{qn} g(t - nT - \tau T)) \exp[j(2\pi f t + \theta)]] + n(t) \quad (8)$$

where $g(t) = g_T(t) \otimes c(t) \otimes f(t)$, $g_T(t)$ is transmitter shaping function, $c(t)$ is channel response, $f(t)$ is prefilter, $n(t)$ is AWGN with two-sided power spectral density $N_o/2$, $a_n \equiv a_m + ja_{qn}$ is data symbol from complex plane ($a_n = A(\pm 1 \pm j)$ for OQPSK signaling, $|a_n|^2 = E_s$). τ is delay factor, which is 0.5 for OQPSK. In our system simulation, we use square root raise cosine shaping filter with rolloff factor equal to 0.25.

2. RCPC Code, Unique Word and Their Performances

A punctured code is a high rate code obtained by periodically deleting (i.e. puncturing) certain coded bits from the output stream of a low rate encoder. When compared with optimum codes of equal rates, punctured codes are slightly less efficient but decoding complexity is greatly reduced. Clearly the puncturing rule determines the receiver structure for different code rates. A family of RCPC codes [16] are generated by adding rate-compatibility restriction to the puncturing rule. The rate-compatible restriction makes the receiver structure nearly identical for a large range of code rates.

From the work in [16], we order the information bits from 11 subbands according to their source significance information (SSI) as $S_{10} \dots S_0$. The ordered information bits are shifted into the shift registers of a $1/N$, memory M convolutional encoder. During the n_{10} information bits from subband 10 the puncturing matrix $a(l_{10})$ (we borrow the syntax used in [16]) is used as puncturing table. As soon as the first bit from subband 9 enters the encoder the puncturing table $a(l_9)$ will be used. After another n_9 information bits, the table is switched to $a(l_8)$, etc. The procedure is easy to follow if n_k is an integer of the puncturing period P .

In order to keep the distortion constant and achieve stable Quality of Service (QoS), the source-coded data is variable bit rate (VBR) information. Some signs should be added in the data stream to inform the receiver the end of each subband. Highly correlated data pattern unique word (UW) is widely used in TDMA systems to identify the start of received bursts. UW could be used here to inform the receiver the beginning of a new subband. The following function is applied for unique word detection:

$$E_{uw} = \sum_{i=1}^n S_i \oplus U_i \quad (9)$$

where \oplus is inverse modulo 2 summation, n is the length of a UW, $S \equiv (S_1, \dots, S_n)$ is received bit after hard-decision, $U \equiv (U_1, \dots, U_n)$ is previously stored UW data pattern. If E_{uw} is larger than some threshold $n - \varepsilon$, the UW is said to be detected. The overall bit error rate upper bound of a rate $P/(P+l)$ convolutional code is given by [17]:

$$P_B < \frac{1}{P} \sum_{k=d}^{\infty} C_k P_k \quad (10)$$

where C_k is got from convolutional code generation

$$\text{polynomial } T(D, N), \left. \frac{dT(D, N)}{dN} \right|_{N=1} = \sum_{k=d}^{\infty} C_k D^k, P_k \text{ is}$$

probability that the wrong path with distance k to correct path is selected. A more relax upper bound for binary symmetric channel (BSC) is given by [16]:

$$P_B < \frac{1}{P} \left. \frac{dT(D, N)}{dN} \right|_{N=1, D=\sqrt{p(1-p)}} \quad (11)$$

where p is the transition probability of BSC. Suppose the UW length n is reasonable long, ε is proper selected, and aperture technique is applied, the UW false detection probability can be omitted. A bit error probability upper bound is:

$$P_B < \sum_{i=0}^{\varepsilon} \binom{n}{i} p^i (1-p)^{n-i} + \sum_{i=\varepsilon+1}^{\infty} \binom{n}{i} p^i (1-p)^{n-i} \frac{1}{P} \sum_{k=d}^{\infty} C_k P_k \quad (12)$$

The first item above is UW miss detection probability. For OQPSK signal over AWGN channel, p is lower

bounded by $Q(\sqrt{\frac{E_s}{N_o}})$. It is easy to achieve this bit error rate with the cutting-edge modem techniques.

If one would like to simplify the system design, constant bit rate (CBR) video stream is also a choice, i.e., each subband has fixed output data length. Only One frame unique word is required to synchronize the whole frame. Figure 4 shows the frame formats for convolutional encoded VBR and CBR video stream.

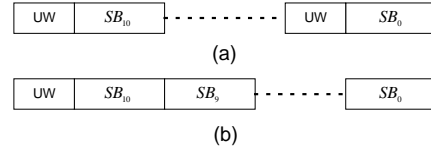


Figure 4 Frame Format (a) VBR (b) CBR

3. Rate Allocation Scheme

In order to optimize the overall subjective video quality at reasonable coding cost, a rate allocation scheme based on JND distortion is proposed. We define the average JND distortion of subband l ($l=0, \dots, 10$) as follows:

$$D_l = \frac{1}{H_l W_l} \sum_{(x,y) \in S_l} JND(x, y)^2 \quad (13)$$

where S_l is the set of pixels of subband l , H_l and W_l are height and weight of it separately. D_l is an indication of the robustness of S_l to errors. The larger D_l is, the more robust it is to errors, the higher coding rate we choose. Table 1 shows D_l for video sequence ‘‘Calendar-Train’’.

l	D_l	l	D_l	l	D_l
0	4.5	4	7.5	8	27.6
1	7.6	5	7.5	9	27.6
2	7.6	6	8.7	10	42.8
3	8.8	7	7.4		

Table 1 Average Distortion D_l for Each Subband

From simulation we can see that D_l divides S_l into four categories, $\{S_0\}$, $\{S_1, S_2, S_3, S_4, S_5, S_7\}$, $\{S_8, S_9\}$, $\{S_{10}\}$, which is intuitive for subband coding.

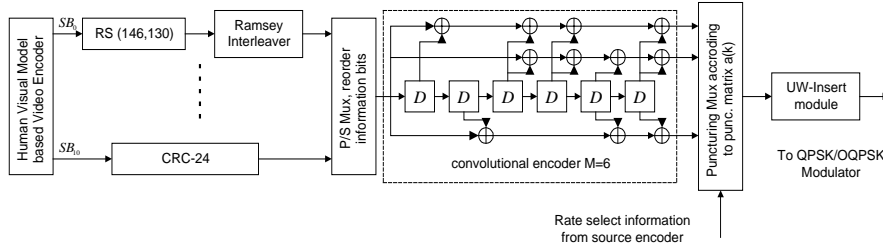


Figure 5 UEP Channel Encoder

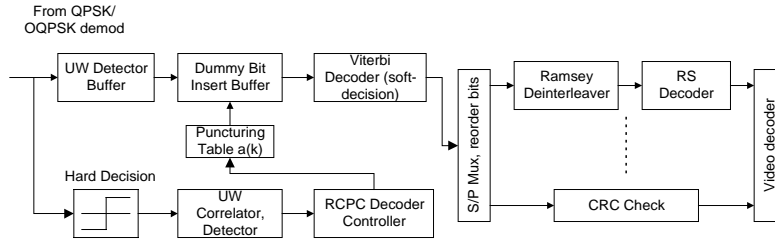


Figure 6 UEP Channel Decoder

4. UEP Channel Encoder and Decoder

Figure 5 shows the unequal error protection (UEP) encoder, Figure 6 shows the corresponding UEP decoder. The spatial LLL temporal L subband (i.e. S_0) is most significant subband, we should use a large amount of our resource to protect it from errors. In order to deal with burst errors in channel Reed-Solomon (RS) code and Ramsey interleaver can be used. After RS encoder, a low rate RCPC code is selected to add more protection. We select a family of RCPC codes (Table II in [15], memory length $M=6$), the coding rate covers from $8/9$ to $8/24$. For other less significant subbands, cyclic redundancy check (CRC) codes are added before RCPC encoder to detect uncorrected errors got from channel. If errors are detected by CRC syndromes check in a block in S_i before arithmetic decoding, we discard this block. Simulation shows that discarding an error-corrupted block is better than using wrong decoded information. Therefore the video quality degradation under bad channel conditions is acceptable if we discard some less important error corrupted subbands because of the performance scalability of wavelet based subband coding. It gives broadcast system designers some freedom to assure the overall video quality without receivers' channel environment information at moderate coding cost.

In decoder, soft-decision (or hard-decision) Viterbi decoder is adopted. An UW detector is used to detect

the start of a new subband. Rate allocation information is available in both sides.

5. Error Concealment in Video Decoder

If errors are detected via CRC decoding in the blocks in subband S_i , these blocks are discarded. If no error is detected, but there are some errors in received sequence, the arithmetic decoder can detect some conflicts during decoding sometimes, therefore find some errors and discard it. In worst that case errors are not detected, they will not spread to the whole subband or the whole frame due to slicing.

III. Simulation Result

Video sequences "Calendar-Train" and "Claire" are used to test our systems. Original frame 1 of "Calendar-Train" and its JND subband profiles are shown in Figure 7. The JND reflects the visual just noticeable distortion for video at a speed of 30 frames/Sec. For example, the calendar part, which comprises of many fine lines and numbers, has smaller values of JND (displayed as smaller gray scale values in (b)) therefore, the distortion is more sensible to human eyes. However, eyes have more tolerance on the distortion at the moving train, which is almost evenly dark.

Figure 8 shows that our distortion measure (4) is better than PSNR in the sense that it reflects the subjective visual quality of image/video better. Figure 8 shows frame 1 in the decoded sequence of "Claire". The PSNR

of (a) and (b) are almost the same, but Δ_G indicates that the distortion of (a) is smaller than that of (b) as we can tell from observation (e.g. shoulder, hair and cheek).

Because the difference between S_{10} and S_8, S_9 is relatively small, we finally assign 11 subbands into three error protection groups: $\{S_0\}$, $\{S_1, S_2, S_3, S_4, S_5, S_7\}$, $\{S_8, S_9, S_{10}\}$.

Index	4	5	6	7	8	9
Rate	8/18	8/16	8/14	8/12	8/10	8/9

Table 2 Rate Index of RCPC

Table 2 shows the coding rate index. The sequence of “Calendar-Train” are coded and transmitted over AWGN channel at different SNR. Figure 9 and Figure 10 show the distortion of first 10 decoded frames with different protection schemes at different SNR (In Figure 9 and Figure 10, the legend 3dB (4,7,8) means that the E_b / N_o is 3dB and we use channel coding rate 8/18 for subband 0, rate 8/12 for subband 1 to 7, and rate 8/10 for subband 8 to 10.)

In Figure 9 the original frames are encoded with the object distortion measure $\Delta_G=1$, which means the compression brings just noticeable distortion in the pictures. Even if the channel is ideal, the distortion Δ_G goes larger gradually ($\Delta_G=1.19$ for Frame 0 and 1.77 for Frame 5) in the following frames. The reason is that the JND model is initially got from the first two frames and is not renewed for the subsequent frames, which brings bias in encoding. The larger the frame number is, the more the bias accumulates

In Figure 10 the original frames are encoded with the object distortion measure $\Delta_G=5$, which means the perceptual distortion is 5 times of the just noticeable distortion. Intuitively, the distortion in Figure 7 should be less than that in Figure 8, however it is not the truth. Because the slices generated by source encoder are longer when $\Delta_G=1$ (finer step size is chosen and more data is transmitted), the probability that a slice is corrupted by errors increases as the number of bits in this slice increases at the same bit error rate (BER). So if a video service requires better quality, the corresponding better channel protection scheme should be chosen.

Figure 11 shows frame no. 3 in recovered sequence of “Calendar-Train”. Some areas corrupted by the channel noise can be observed.

IV. CONCLUSION

We present a satellite video transmission system based on wavelet analysis and human vision model. The joint source channel coding scheme is investigated. We propose a new performance index based on the JND model. The quantizer and slicer are perceptually optimized. Since we focus on subjective quality and error concealment, more powerful compression schemes (e.g. zero-tree, motion estimation and run-length coding) are not applied in our system.



(a)



(b)

Figure 7 (a) Frame 1 of “Calendar-Train”(b) JND Subband Profile for Subband 0 to 6



Figure 8-a Decoded Frames of “Claire”, $\Delta_G=2.38$, PSNR=30.80dB



Figure 8-b Decoded Frame of “Claire”, $\Delta_G=3.07$, PSNR=30.15dB

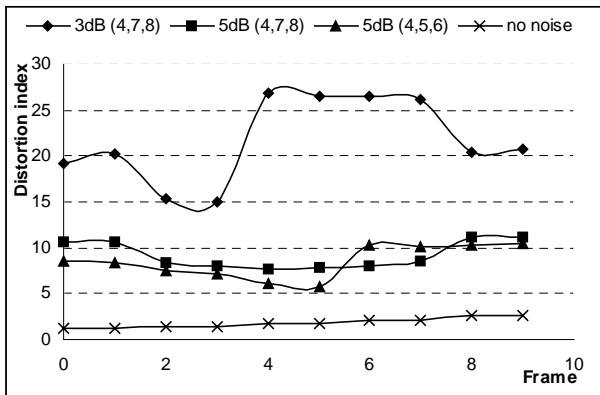


Figure 9 Distortion Δ_G of the Decoded Frames over Noisy Channel with object distortion index 1

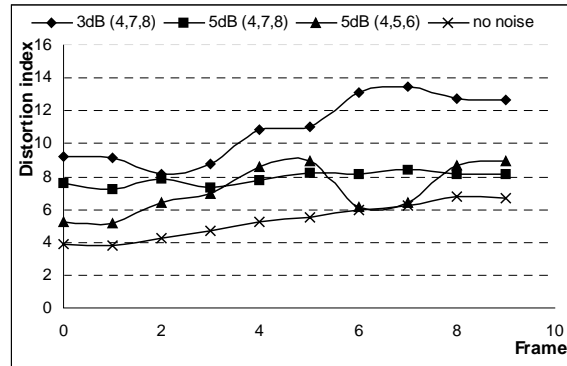


Figure 10 Distortion Δ_G of the Decoded Frames over Noisy Channel with object distortion index 5



Figure 11 Decoded Frame 3 of “Calendar-Train” with $E_b/N_o = 3dB$ (4,7,8) protection

Reference:

1. Taubman and A. Zakhor, “Multirate 3-D subband coding of video”, *IEEE Trans. Image Processing*, vol. 3, pp572-588, Sept. 1994.
2. C. Podilchuk, N. Jayant and N. Farvardin, “Three-dimensional subband coding of video”, *IEEE Trans. Image Processing*, vol. 4, pp125-139, Feb. 1995.
3. D. Taubman, “Directionality and scalability in image and video compression”, *Ph.D. dissertation*, Univ. California, Berkeley, 1994.
4. J. Y. Tham, S. Ranganath and A. Kassim, “Scalable low bit rate video compression using motion compensated 3-D wavelet decomposition”, in *IEEE ICCS/ISPACS 1996*, vol. 3, pp39.7.1-39.7.5, Nov. 1996.
5. N. Jayant, J. Johnston and R. Safranek, “Signal compression based on models of human

- perception”, *Proc. IEEE*, vol. 81, pp1385-1422, Oct. 1993.
6. C. H. Chou and Y. C. Li, “A perceptually tuned subband image coder based on the measure of just-noticeable-distortion profile”, *IEEE Circuits and Systems for Video Tech.*, vol. 5, pp467-476, Dec. 1995.
 7. C. H. Chou and C. W. Chen, “A perceptually optimized 3-D subband codec for video communication over wireless channels”, *IEEE Circuits and Systems for Video Tech.*, vol. 6, pp143-156, April 1996.
 8. S. Daly, “The visible differences predictor: an algorithm for the assessment of image fidelity” in *Measurement and Prediction of Visual Quality*.
 9. X. Ran and N. Farvardin, “A perceptually motivated three-component image model - Part I: Description of the model”, *IEEE Trans. Image Processing*, vol. 4, pp401-415, April, 1995.
 10. M. Antonini, M. Barlaud, P. Mathieu and I. Daubechies, “Image coding using wavelet transform”, *IEEE Trans. Image Processing*, vol. 1, pp205-220, April 1992.
 11. D. H. Kelly, “Motion and vision II. Stabilized spatio-temporal surface”, *J. Opt. Soc. Amer.*, vol. 69, pp1340-1349, Oct. 1979.
 12. N. Jayant, “Signal compression: Technology targets and research directions”, *IEEE JSAIC*, vol. 10, pp796-818, June 1992.
 13. N. Farvardin and J. Modestino, “Optimum quantizer performance for a class of non-Gaussian memoryless source”, *IEEE Trans. Information Theory*, vol. 30, pp485-497, May 1984.
 14. I. Witten, R. M. Neal and J. G. Cleary, “Arithmetic coding for data compression”, *Comm. of the ACM*, Vol. 30, pp520-540, June 1987.
 15. N. Chaddha, S. Diggavi, “A Frame-work for Joint Source-Channel Coding of Images over Time Varying Wireless Channels ”, *Proc., International Conference on Image Processing*, 1996.
 16. J. Hagenauer, “Rate-Compatible Punctured Convolutional Codes (RCPC Codes) and Their Application ”, *IEEE Trans. Comm.*, April 1988, vol. 36, no.4, pp. 389-400.
 17. A. J. Viterbi, “Convolutional Codes and Their Performance in Communication Systems ”, *IEEE Trans. Comm.*, Oct., 1971, vol. COM-19, no. 5, pp. 751- 772.